Attaining High Signal-to-Noise Data with the Goddard High Resolution Spectrograph

Jason A. Cardelli[1] and Dennis C. Ebbets[2]

Abstract

We present an analysis of the characteristics of fixed pattern noise and photocathode granularity in the detector system of the Goddard High Resolution Spectrograph and the impact this noise can have on science data. We show that through the application of some basic and straightforward observing and data reduction techniques, this instrumental noise can be effectively suppressed, allowing high signal-to-noise (S/N) data to be achieved. Using these techniques, numerous examples of spectra with S/N ≈ 300 – 1000 have thus far been obtained. Analysis of the noise characteristics of these high S/N spectra also show the data to be essentially at the photon-limit.

I. Introduction

The high resolution (3.5 km/sec) and linear photon-counting detector capabilities of the Goddard High Resolution Spectrograph (GHRS) offer a fantastic opportunity to obtain superb spectroscopic data, unprecedented in the history of satellite UV spectroscopy. However, as is the case with many detector systems, especially those employing photocathodes, the detector system of the GHRS is plagued by fixed pattern noise. The presence of such noise effectively limits the signal-to-noise (S/N) that can obtained in a single exposure at a fixed grating position. While the GHRS detector system noise does not inhibit work on moderate-to-strong absorption lines (i.e., > 10 percent deep), its effects can be devastating for weak lines (< 5 percent deep). Weak line work is important because it provides a unique opportunity to study weak transitions from important abundant species (Cardelli et al. 1991; Cardelli et al. 1993b; Cardelli and Ebbets 1994) as well as the strongest transitions from species with very low cosmic abundance (Cardelli, Ebbets, & Savage 1991; Cardelli et al. 1993a; Hobbs et al. 1993; Federman et al. 1993).

In this paper we present an analysis of fixed pattern noise and its potential impact on science data. We show examples of its variability with wavelength and how the analysis of the noise characteristics can be affected by such things as Doppler compensation. We also provide a generalized discussion of some simple and straightforward observing and data reduction techniques that can be used to suppress fixed pattern noise and granularity to below that of the photon noise.

1. Department of Astronomy, University of Wisconsin, Madison, WI 53706
2. Ball Aerospace Research Group, Boulder, CO 80306

II. Fixed Pattern Noise/Photocathode Granularity

General Characteristics: Side 1 and 2

The noise in the GHRS detector system arises from two major sources: 1) fixed pattern noise features resulting from scratches and manufacturing marks present in the photocathode window and 2) granularity and non-uniformities in the photocathode. Additional contributions arise from particulate contamination. Examples of the detector system noise are shown in Figure 1 for side 1 (CsI photocathode deposited on a LiF window) and side 2 (CsTe photocathode deposited on a MgF_2 window) detector systems. The data were obtained with G140M and G160M using STEP–PATT=4 which produces 2 samples (pixels) per science diode. As seen in the figure, with the exception of a few notable broad and deep features, the fixed pattern noise features are generally narrow and have a typical depth of a few percent. The photocathode granularity is much less pronounced, being characterized by weak oscillations typically ≤ 1 percent in depth. The S/N values correspond to expected values from photon statistics. The data are of such high quality that essentially every feature seen in the spectra can be attributed to detector system noise.

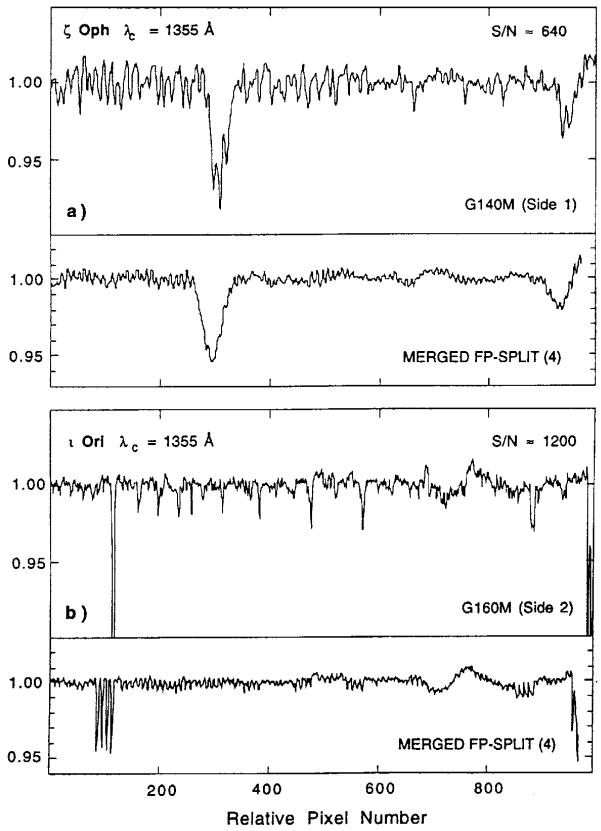

Figure 1: Examples of fixed pattern noise/photocathode granularity spectra derived from data obtained at a setup wavelength of 1355 Å for **a**) G140M (side 1) data of ζ Oph and **b**) G160M (side 2) data of ι Ori. The S/N values listed represent the values expected from photon statistics. Consequently, essentially all the structure seen in the noise spectra result from fixed pattern and photocathode granularity sources. The bottom panels in both **a**) and **b**) show how the noise would impact science data if the FP–SPLIT subexposures were simply aligned and merged in wavelength space.

Wavelength-Dependence

Scratches, blemishes, and non-uniformities in the GHRS detector system are geometrically distributed throughout the 2-dimensional detector window. Consequently, specific noise features present in any observation will be a function of where the spectrum falls on the window. For first order gratings, the spatial location of the spectrum in the direction perpendicular to the dispersion (Y-position) is relatively well fixed, ignoring thermal and magnetic drifts. However, in the echelle modes, each order will have a different Y-position and so the noise structure may change dramatically from one order to the next (different orders are observed by magnetic deflection onto the Digicon detector).

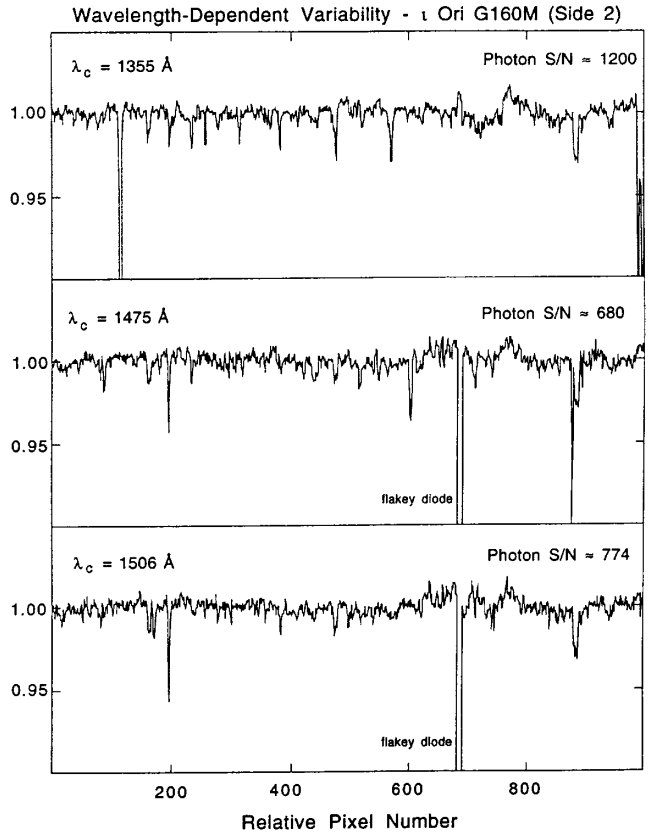

Figure 2: Examples showing the variability exhibited by fixed pattern noise as a function of wavelength for data of ι Ori obtained with grating G160M (side 2) at 1355 Å, 1475 Å, and 1506 Å. The S/N values shown have the same meaning as in Figure 1. The bottom two panels indicate that even relatively small changes in the setup wavelength can have profound effects on the noise spectrum.

Figure 2 shows an example of noise spectra obtained at three different setup wavelengths from G160M data of ι Ori. The data were obtained with STEP–PATT=4. Close examination shows that with few exceptions (e.g., the broad noise feature near pixel 900) the noise features show considerable variation with wavelength with some varying in strength (e.g., the feature near pixel 200) and others appearing in only one of the spectra (e.g., the feature near pixel 600). Sources of this variation may include wavelength sensitivity of the noise features, Y-position displacement of the spectrum from one wavelength setup to the next, or particulate contamination.

III. Noise Assessment

Suppression / Removal Procedures

For an observation obtained at a single grating setup position, the data in Figure 1 show that the best one could possibly hope to do (in regions away from the strong noise features) is about S/N ≈ 50 on either side 1 or 2. When the GHRS commanding was designed, an optional procedure called FP–SPLIT was created to specifically to deal with the presence of noise structure.[1] This procedure breaks each requested observation into a number of subexposures (the default is 4), each obtained at a slightly different grating tilt which shifts spectral features relative to the fixed pattern noise. When individual subexposures are aligned in wavelength space, the noise features in each subexposure are offset by about 4.5 diode widths. When the data are merged, the impact of the noise is significantly reduced, as seen in the bottom panels in Figure 1. However, the maximum S/N is still restricted to values less than about 150.

To achieve significantly higher S/N values, one must effectively derive a flat-field template which can be used to significantly reduce the noise structure to at or below that of the photon noise. The procedure we have adopted is shown in a flow chart in Figure 3. It involves an iterative procedure in which 1) a spectrum template is determined by aligning the spectral features and combining the subexposures, 2) the spectral template is divided into the original subexposures, 3) a noise template is determined by aligning the noise features and combining the subexposures, 4) the noise template is divided into the original subexposures, and 5) the process repeats with step 1). This procedure works because in each subexposure, there is a different offset between any particular spectral and noise feature.

An example of the application of the procedure outlined in Figure 3 is shown in Figure 4 for data of ι Ori. The first three spectra show the derived noise template, the raw (uncorrected), and the corrected data for the first (left panel) and fourth (right panel) FP–SPLIT subexposure, plotted against pixel number. Note that between the two subexposures, the spectral features have moved in pixel (detector) space while the noise features have stayed essentially fixed in pixel space. Note how well the strong noise features are removed when the data are divided by the template (the same is found for the other 2 FP–SPLIT subexposures). The bottom two spectra are the same in each panel and represent, 1) addition of the four corrected FP–SPLIT subexposures and 2) addition of four separate observations (16 FP–SPLIT subexposures). The S/N values listed were empirically derived from the continuum and are essentially the same as what is predicted from photon statistics.

The Impact of Doppler Compensation

For the small wavelength shifts produced by the procedure FP–SPLIT, no significant change in the noise structure is seen and all noise features should appear fixed in pixel (diode) space. However, because the velocity of the spacecraft relative to the target changes due to orbital motion, a spectrum obtained at some arbitrary grating

1. See GHRS Handbook for a discussion of FP-SPLIT and other instrumental settings.

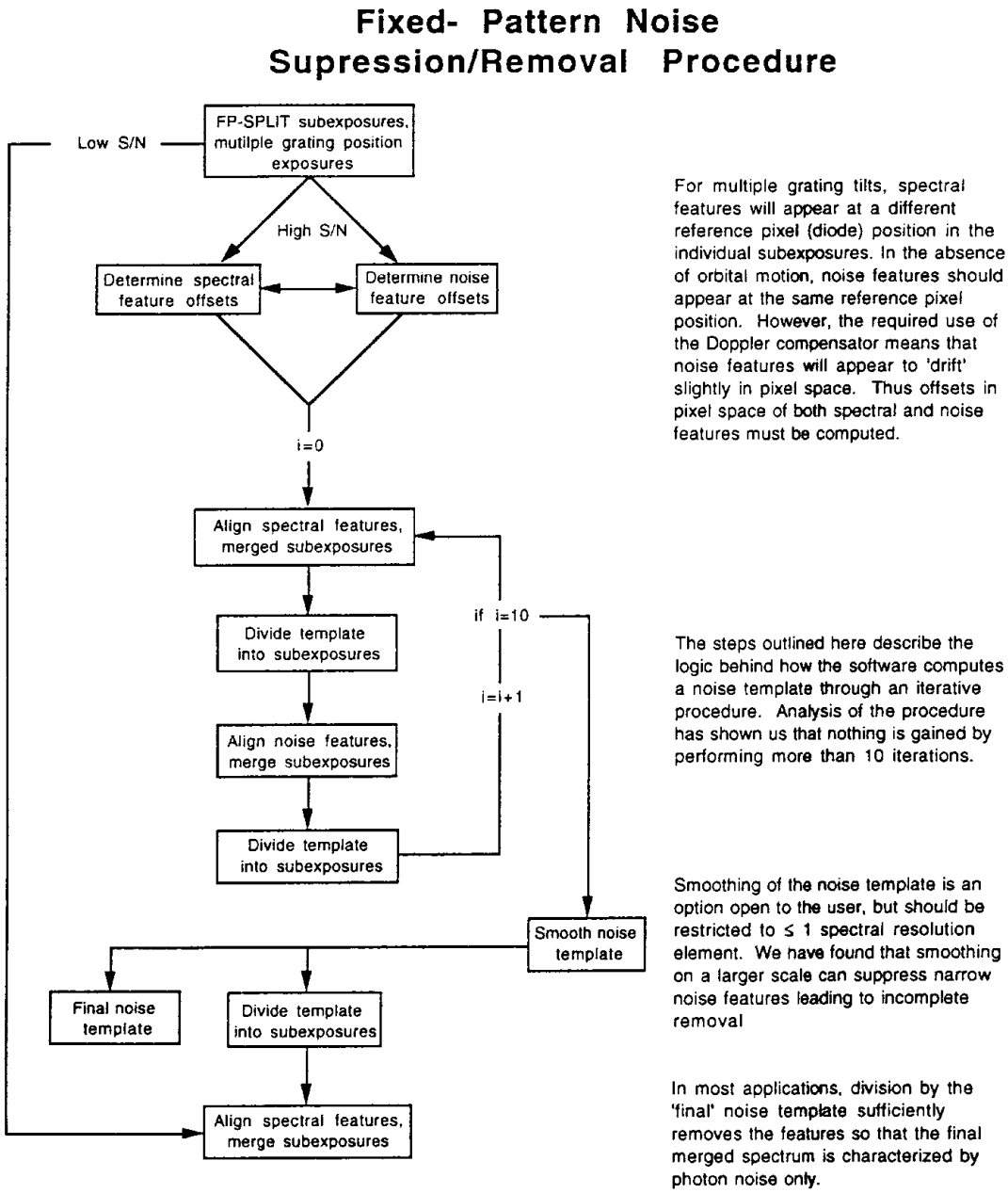

Figure 3: A flow chart showing the logical steps involved in processing GHRS data for fixed pattern noise. The low S/N channel can be applied in cases where the desired spectral feature is in a region characterized by 2 – 3 percent deep features *only* and the maximum S/N expected from photon statistics is < 150 (see the bottom panels in Figure 1).

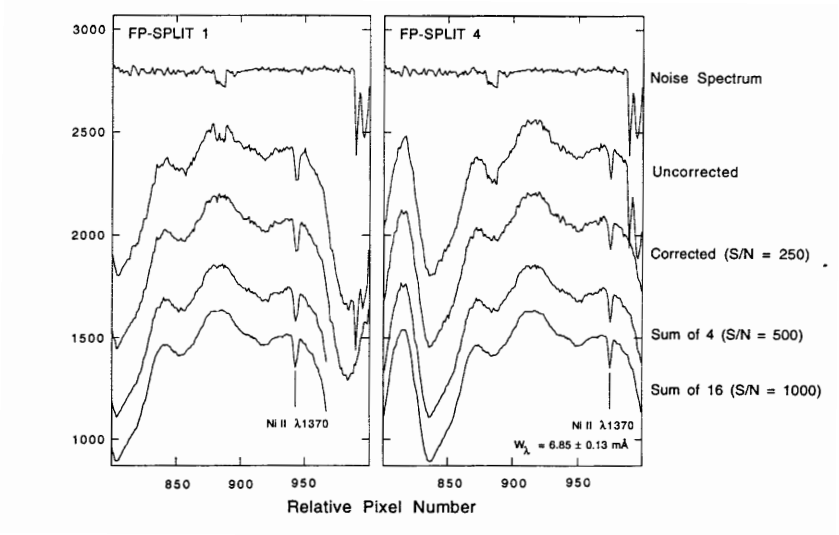

Figure 4: An example of the removal of fixed pattern noise from a portion of 2 FP–SPLIT subexposures of ι Ori. The noise template was determined using the steps outlined in Figure 3. The effects of the major noise features are clearly seen in the raw (uncorrected) spectra. The corrected spectra result from dividing the derived noise template into the raw (uncorrected) spectra. The sum of 4 spectra correspond to the merging of the four noise-corrected FP–SPLIT subexposures. The bottom spectra result from merging four separate observations (total of 16 FP–SPLIT subexposure). The S/N values were empirically derived from the continuum and are essentially the same as what is expected from photon statistics.

position can shift by a maximum of ±8 km/sec in 80 minutes (about ±1/2 diode in intermediate resolution and about ±2.3 diodes in high resolution). Since each subexposure is broken into many individual integrations which are dumped into the on-board accumulator bins, the Doppler compensator is used to apply the velocity shifts to each spectral integration prior to it being stored so that the spectral features do not become smeared in wavelength space. In addition to producing a small smearing of the noise features in each subexposure, comparison of the individual subexposures shows that the noise features can exhibit some drift in pixel space (in deriving the noise template, drifts of the noise structure in pixel space are accounted for in the reduction procedure – see Figure 3). This drift is most pronounced in the high resolution echelle mode. An example of this is shown in Figure 5 for Echelle–B data of ζ Oph in the neighborhood of a strong interstellar Mn II line. The movement of the spectral line between the FP–SPLITs (and relative to the noise structure) in pixel space is the result of different grating tilts and serves as the basis by which the noise template is derived.

In addition to a small and steady drift in time (the time sequence of the observations runs from top to bottom), the noise features in Figure 5 also show a sudden and substantial jump between the third and fourth subexposure (at FP–SPLIT position no. 2). This jump resulted from a long orbital interrupt of the observing sequence. When the exposure resumed, the velocity of the spacecraft relative to the star had changed by –10.5 km/sec. Had the interrupt occurred *between* subexposures, all of the data would be usable. Unfortunately, the interrupt came with 20 percent of the time remaining on subexposure 3. When the observation continued, the noise features were shifted by –10.5 km/sec which resulted in a significant degradation of

the noise structure in this subexposure relative to the others as can be seen in an examination of the data in panel b).

The data in subexposure 3 cannot be used in deriving the noise template and probably should not be used in the merged spectrum, especially if a major goal is to search for weak lines. In this case we have not lost much since it is only one of eight subexposures. However, the consequences would have been more serious had we only obtained one exposure in each FP–SPLIT position. Fortunately, this problem does not occur very often.

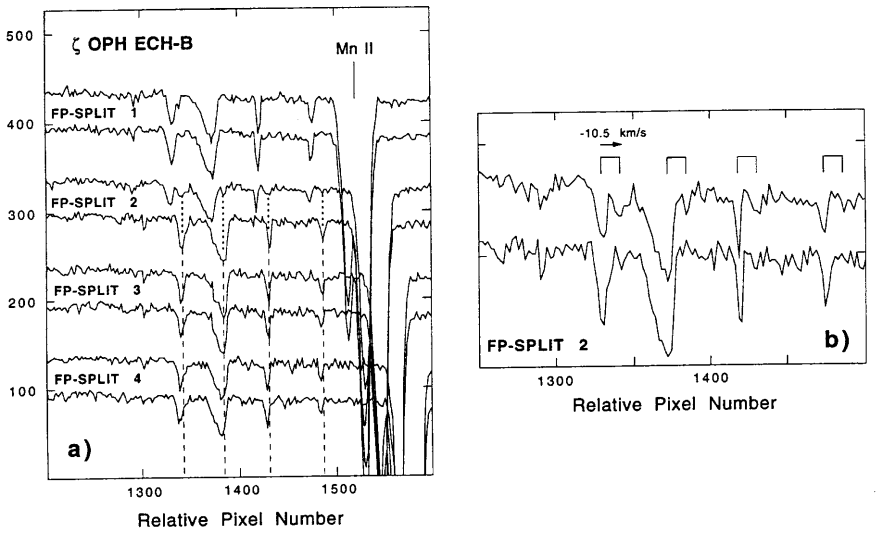

Figure 5: A portion of an echelle–B observation of ζ Oph in the neighborhood of a strong interstellar line of Mn II, plotted in pixel space, is shown in panel a). The data were obtained with two subexposures at each of the four FP–SPLIT positions using STEP–PATT=7 (four samples per diode). The apparent movement of the fixed pattern noise features in pixel (detector) space is the result of the Doppler compensator. The jump in the features between subexposures 3 and 4 result from an orbital interrupt prior to the completion of subexposure 3. Panel b) shows that the subexposure resumed at a point in the orbit when the component of the orbital motion in the direction of the star had changed by –10.5 km/sec.

High Signal-to-Noise Science Data

To date, the techniques outlined here have been used on data obtained in a number of different programs to produce high quality spectra with $300 \leq S/N \leq 1200$. Some examples of results produced for weak absorption lines are shown in Figure 6. The S/N values were measured from the continuum and are consistent with the data being in the photon limit.

Residual Noise Characteristics

Our statement that our results are essentially in the photon-limit derives from the fact that the empirical S/N values are the same as those obtained from $(\text{total counts})^{1/2}$. To explore this further, it is useful to actually examine the noise structure to see if it behaves according to Poisson statistics (e.g., the noise is characterized by a

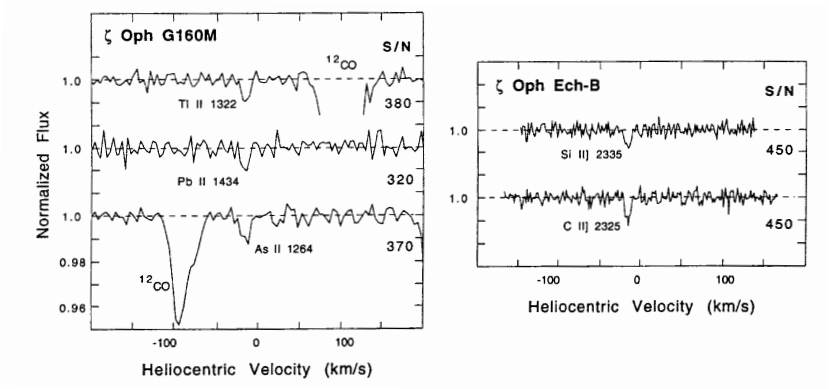

Figure 6: Selected examples of weak lines observed in high S/N Data of ζ Oph using both G160M (with four samples/diodes) and Ech–B (with two samples/diode). The S/N values were empirically derived from the continuum and are consistent with what is expected from photon statistics. The data are taken from: Tl II and Pb II (Cardelli & Ebbets 1994); as II (Cardelli et al. 1993a); C II] (Cardelli et al. 1993b); Si II] (Cardelli et al. 1994).

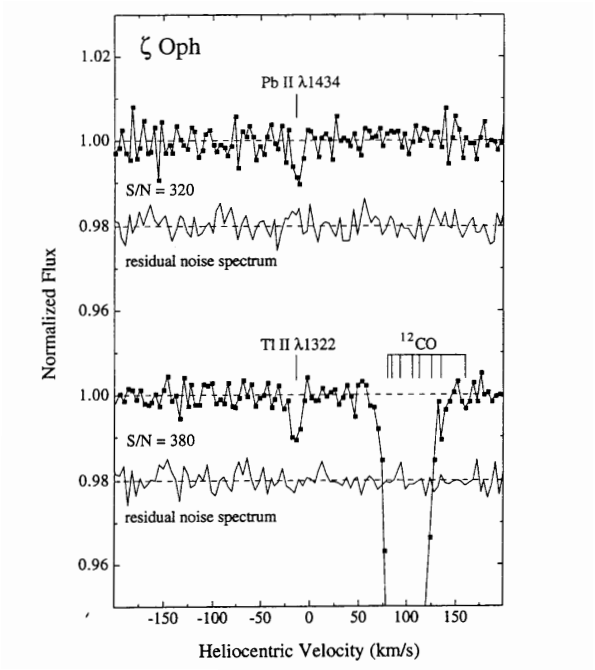

Figure 7: The weak lines of Tl II and Pb II observed toward ζ Oph (Cardelli & Ebbets 1994). The data labeled residual noise spectrum were derived by taking the noise-corrected subexposures and running them through the noise extraction routines outlined in Figure 3 for the purpose of determining if residual noise structure is present. No such structure is present and the S/N of these data are the same as the reduced spectra which is essentially the same as that expected from photon statistics.

Gaussian distribution). As a start, we explore how well our noise extraction routines suppress the noise. An example is shown in Figure 7 for the weak line data of Tl II and Pb II obtained toward ζ Oph (Cardelli & Ebbets 1994). The lower plot marked residual noise spectrum was determined by running the noise corrected subexposure back through the noise extraction routines outlined in Figure 3. Had our original noise template not sufficiently removed the noise structure (such as would be the case

for the data in Figure 5), we expect that some residual noise structure would be present. However, we see no evidence for this in the data. In fact, the empirical S/N measured in the residual noise spectrum is the same as that for the actual data. This result also gives us confidence that the features we observe are real.

A more definitive method is to explore the nature of the noise distribution about the fitted continuum. For this we use the ζ Oph C II] λ2325 Å data (Cardelli et al. 1993b) obtained with Ech–B. These data are particularly useful because the continuum in this spectral region is relatively flat and featureless which minimizes possible continuum fitting uncertainties. The distribution of the noise about the fitted continuum is shown in Figure 8. Also shown is a fit of a Gaussian function to the data. The Gaussian nature of the noise distribution coupled with the fact that the measure S/N is the same as that obtained from (total counts)$^{1/2}$ gives us confidence that the spectrum is dominated by photon noise. (A similar analysis of the data in Figure 7 yields similar results.)

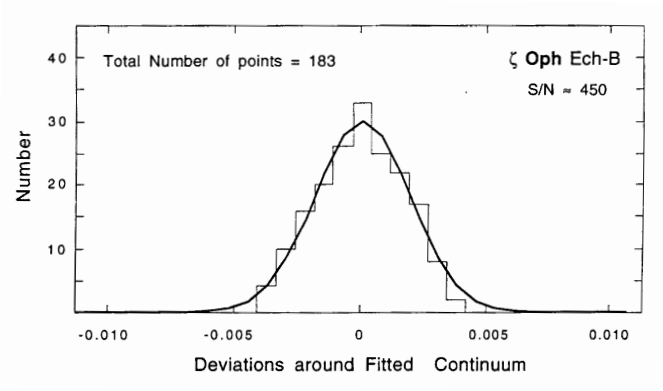

Figure 8: An example of the noise distribution about the fitted continuum of the noise-corrected C II] λ2325 Å (Cardelli et al. 1993b) shown in Figure 6. As can be seen, the data are consistent with a Gaussian distribution indicating that the data are well represented by Poisson statistics. This quantitatively supports our contention that the empirically derived S/N is consistent with what is expected from photon statistics.

IV. Recommendations

The techniques outlined here have proven to be highly robust in a number of applications and numerous examples of high S/N results have been published. However, as shown in Figure 5, there are cases where problems do arise. If the desired goal of an observer is to obtain high S/N to measure weak lines or simply to obtain the best possible data, this will be best accomplished if some basic steps are followed. We therefore offer some suggestions and recommendations to ensure the best results.

- Always use the FP–SPLIT option, even if the expected S/N is relatively low. Some noise features are quite strong (see Figure 1) and could corrupt your data.
- Break an observation into multiple exposures to avoid serious data loss due to the possible consequences of orbital interrupts. This also decreases the photon noise contribution of the noise template relative to the individual subexposure.

- For high S/N work, also obtain multiple grating position observations at intervals of 0.5 – 1 Å using FP–SPLIT at each setup wavelength. This will give you a larger baseline from which to derive a noise template and will also increase the randomization of any residual noise features in the final merged spectrum.
- Try to limit the exposure time per readout to ≤ 4 minutes. This will decrease the chance of losing data to glitches and will lower the probability of problems associated with orbital interrupts. This also reduces the amount of smearing of the noise features due to Doppler compensation.
- Since the effects of orbital motion produce at most a maximum shift of 1 diode in the intermediate resolution modes, it may be useful to disable the Doppler compensator in the case of weak line work (i.e., where there is more interest in the measurement rather than the profile). This will eliminate the problem of noise feature drifts in pixel space. This is NOT recommended for observations obtained with the echelle modes.
- For intermediate resolution modes, the best results are obtained using STEP–PATT=5 (four samples per diode), especially for weak lines. For the echelle modes, two samples per diode (STEP–PATT=6) will suffice, but four samples per diode (STEP–PATT=7) should be obtained if time permits.
- Limit the smoothing of the noise template to ≤ 1 resolution element (one diode). While some smoothing may be necessary to minimize photon noise contributions relative to the individual subexposures, the noise features are not imaged by the gratings and so they are potentially resolvable on scales smaller than the resolution element. Too much smoothing can produce residual noise pings that can appear in the final merged spectrum.

References

Cardelli, J. A., & Ebbets, D. C. 1994, in preparation

Cardelli, J. A., Federman, S. R., Lambert, D. L., & Theodosiou, C. E. 1993a, ApJ, 416, L41

Cardelli, J. A., Mathis, J. S., Ebbets, D. C., & Savage, B. D. 1993b, ApJ, 402, L17

Cardelli, J. A., Savage, B. D., & Ebbets, D. C. 1991, ApJ, 383, L23

Cardelli, J. A., Sofia, U. J., Savage, B. D., Keenan, F. P., and Dufton, P. L. 1994, ApJ, in press.

Federman, S. R., Sheffer, Y., Lambert, D. L., & Gilliland, R. L. 1993, ApJ, 413, L51

Hobbs, L. M., Welty, D. E., Morton, D.C., Spitzer, L., & York, D. G. 1993, ApJ, 411, 750

Lambert, D. L., Sheffer, Y., Gilliland, R. L., & Federman, S. R. 1994, ApJ, in press

Sheffer, Y., Lambert, D. L., Federman, S. R., & Cardelli, J. A. 1992, ApJ, 397, 482

Editors' Note: A paper was also given by these authors, and presented by Dennis Ebbets, entitled "Calibration and Removal of Scattered Light in the Echelle Modes of the GHRS." A full description of the study appears in the following two published papers: Cardelli, Ebbets & Savage, 1990, ApJ, 365, 789; and Cardelli, Ebbets & Savage, 1993, ApJ, 413, 401.